Methane adsorption on carbonaceous microporous materials prepared from cellulose and lignin: Equilibrium and kinetic studies

S. Pourebrahimi[a], M. Kazemeini[a,*], M. Zaroudi[a], and H.R. Bozorgzadeh[b]

a. *Department of Chemical and Petroleum Engineering, Sharif University of Technology, Tehran, P.O. Box 11365-9465, Iran.*
b. *Gas Division, Research Institute of Petroleum Industry, West Blvd. of Azadi Sports Complex, Tehran, P.O. Box 18745-4163, Iran.*

Abstract. The present investigation highlights methane adsorption on synthesized Activated Carbons (ACs) based upon hydrothermally treated cellulose and lignin followed by chemical activation utilizing $ZnCl_2$ as the activating agent. The influence of effective parameters such as hydrothermal pretreatment, precursor type, carbonization temperature, and impregnation ratio on the textural properties of synthesized materials as well as adsorption capacities of methane was examined. Thermal stability and decomposition procedures of cellulose and lignin were determined through the TGA technique while all prepared ACs were characterized via N_2 adsorption-desorption analysis utilizing BET-BJH surface area measurement and Field Emission Scanning Electron Microscopy (FESEM). Amongst all prepared materials, the AC that was produced through impregnating hydrothermally treated cellulose with $ZnCl_2$ with the ratio of 1 and carbonized at $600°C$ revealed improved surface and textural properties and enhanced methane storage. Furthermore, hydrothermal pretreatment provided micro-pore diameters ranging from 1.8 to 2.2 nm. This resulted in 6.42 mmol.g^{-1} of methane adsorbed at 298 K and 3.65 MPa. In order to systematically understand behaviors of adsorbents in the process at hand, several kinetic and isotherm models were investigated.

1. Introduction

Natural Gas (NG) is considered to be an important energy supply and a non-renewable source being inexpensive and abundantly available in the present world. The major problem of using the NG as fuel is believed to be its low energy density. The most common way of its storage for achieving high energy density is compression at high pressures (i.e., up to 20 MPa) while maintaining it in special vessels. Surely, this leads to high cost, which is considered to be the main disadvantage of this technique. On the other hand, a well-known alternative to this is the Adsorbed Natural Gas (ANG) technique. The advantage of utilizing this latter method is attributed to lowering the pressure (i.e., to 2-4 MPa), hence, reducing cost of storage [1]. In the ANG technique, a lightweight storage tank might be filled with a highly porous adsorbent using an inexpensive single-stage compressor.

A good carbon adsorbent for natural gas storage

*. *Corresponding author. Tel.: +98 21 66165425;*
Fax: +98 21 66012983
E-mail addresses: sina.pourebrahimi@gmail.com (S. Pourebrahimi); kazemini@sharif.edu (M. Kazemeini); Maryzrd@gmail.com (M. Zaroudi); bozorgzadehhr@ripi.ir (H.R. Bozorgzadeh)

should possess: (i) high micro-porosity (i.e., pores with sizes below 2 nm) for storage of small molecules like methane, (ii) low bulk density, to have high volumetric storage capacity, and (iii) high specific surface area with reactive-adsorptive sites for efficient adsorption [2]. Some adsorbents used for NG storage include zeolites [3], carbon nanotubes [4], and metal-organic frameworks [5,6]. In addition, in many cases, Activated Carbons (ACs) [7] demonstrate higher volumetric adsorption besides being simpler and having less expensive preparation procedures [8]. Extensive research has been carried out to explore applications of ACs for the NG storage purposes [9,10].

Chemical activation with different agents including KOH, NaOH, H_3PO_4, and K_2CO_3 as well as physical activation with CO_2 and steam has been applied for preparing the AC materials. By using chemical activation instead of the physical one, energy consumption and operating cost decrease; meanwhile, carbon yield increases and large micro-pore volume and surface area are obtained. Furthermore, the former activation leads to better porous structure than the physical one does [11]. Lignin and cellulose are carbon-rich and potentially available materials; hence, their transformation into ACs is considered to be economically feasible [12] while providing proper textural characteristics. Studies on the ACs produced from the lignin and cellulose indicate that carbon content of lignin is higher than that of cellulose; thus, the micro-pore volume of the AC produced from the former is higher than that from the latter [13]. On the other hand, the content of hydroxyl groups in the structure of cellulose is higher than that in lignin, causing creation of higher total pore volume and specific surface area in the structure of the produced AC [14]. In addition, utilizing hydrothermal carbonization (HTC) processes for producing ACs has recently been reported [15]. HTC, a wet thermal process, takes place at low temperatures (180-300°C) in a closed system under relatively high pressure. During carbonization, a series of reactions occur, leading to generation of a carbon-rich, high energy and density material referred to as hydrochar [16]. This results in incipient porosity and a special morphology, making it a suitable precursor for producing ACs [17]. Hence, the AC prepared in this manner has a well-defined micro-porous structure with high pore volume, specific surface area, and good yield.

Recently, a researcher produced a nano-structured activated carbon with a high specific surface area (1700 $m^2.g^{-1}$), large pore volumes (composed of micro- and meso-pores equal to 0.79 $cm^3.g^{-1}$), and an average pore diameter of 1 nm through hydrothermal pretreatment of hazelnut shells activated with the KOH solution [18]. In another work done, ACs were prepared from lignocellulosic materials by hydrothermal pretreatment followed by physical activation [19]. The resulting hydrochars had a weak porous structure with low-quality surface chemistry. However, activation with CO_2 developed a micro-porous structure with a BET surface area of up to 438 $m^2.g^{-1}$.

In the present study, samples of activated carbons were prepared from hydrothermally pretreated cellulose and lignin using $ZnCl_2$ as an activating agent. Effects of the hydrothermal process and variable parameters such as impregnation ratio and carbonization temperature on textural and chemical-surface properties as well as methane storage capacities of the products were examined.

2. Experimental

2.1. Materials
The microcrystalline cellulose used in this work was obtained from the Merck Chemical Company (product#102331 with molecular formula of $(C_6H_{10}O_5)_n$). Elemental analysis of this white powder carried out by the vendor revealed C = 44 wt%, H = 6 wt%, and O = 50 wt%. The lignin with the molecular formula of $(C_9H_{10}O_2)_n$ used in this work was a brown powder purchased from the Sigma-Aldrich Inc. (product#471003 with low sulfonate content of 4wt%). Elemental analysis of this powder performed also by the vendor showed C = 61.4 wt%, H = 4.9 wt%, ash = 0.7 wt%, and O = 29 wt%. The activating agent of $ZnCl_2$ (50 wt%) was purchased from the Merck Chemical Company (product#108816).

2.2. Synthesis of activated carbons
The hydrothermal pretreatment of raw cellulose and lignin was carried out through the following procedure. At each run, 10 g of raw material was mixed with 50 mL of deionized water and then, transferred into a stainless steel autoclave with removable internal cylindrical Teflon. Filling factor of the autoclave was about 0.83. Then, the autoclave was placed in a furnace maintained at 250°C and equilibrated pressure of ≈ 2 MPa (i.e., a mild set of hydrothermal condition) for 3 h. Afterwards, this was left to quench at room temperature. The solid product of this treatment, referred to as the hydrochar, was separated from its surrounding liquid through filtration and washed thoroughly with distilled water. Finally, it was dried at 120°C for 6 h in an oven. Next, the dried hydrochar was impregnated with the 50 wt% solution of $ZnCl_2$ activating agent at agent/precursor impregnation ratios of 0.5, 1, and 1.5. The impregnated samples were dried at 120°C for 24 h. Then, carbonization was carried out at 500, 600, 700, and 800°C under constant N_2 flow of 250 mL/min. The heating rate applied was 4°C/min and the carbonization time was set to 60 min. All products were ultimately washed thoroughly with distilled water and HCl. The resulting

activated carbon was dried overnight. In addition, two samples were produced from cellulose and lignin without the aforementioned hydrothermal treatment.

2.3. Characterization

The thermal stability analysis of lignin and cellulose was performed through Thermo-Gravimetric Analysis (TGA) technique (Mettler Toledo 851 analyzer). Samples were heated from the room temperature to 800°C with a rate of 10°C/min in a nitrogen atmosphere at a flow rate of 15 mL/min. The initial mass of every sample was 0.5 g at each run. The textural properties of the prepared ACs were characterized with a gas sorption analyzer (Micromeritics 2020 ASAP analyzer). BET surface area, pore volume, micro-pore volume, and average pore diameter were determined through nitrogen adsorption-desorption isotherms at 77 K (i.e., the BET-BJH surface area measurement). The FESEM images were obtained by a field emission scanning electron microscope (HITACHI S-4160) to explore the morphologies of the synthesized samples.

2.4. CH₄ adsorption measurements

2.4.1. Adsorption isotherms of CH₄ on the samples

In order to examine the CH_4 adsorption capacities of the prepared adsorbents, an in-house-made volumetric apparatus was used under equilibrium conditions. The utilized rig had been provided in a previous publication by this research group [20].

2.4.2. Obtaining experimental adsorption kinetic data

To investigate the time dependency of the CH_4 adsorption upon the synthesized sorbents, pressure of the adsorption column was recorded at every 10 s interval until the adsorption system reached equilibrium. At that point, the pressure of the adsorption column became constant. Thus, through specifying the initial adsorption column pressure, one might calculate the adsorbed amounts of the CH_4 at different time intervals, leading to kinetic evaluations of the system.

2.4.3. Methane adsorption calculations

To determine the amount of adsorbed methane, the dead volume measurement was crucial. It investigated the macro- and meso-pores through which methane adsorption might not take place and was performed by helium injection. The volumes of helium penetration into gas tank and the sample cell were assumed to be V_1 and V_2, respectively. The former (i.e., V_1) was calculated using the initial pressure in the gas tank (P_1) and V_2 was the total volume calculated at the equilibrium pressure of the entire system (P_2). The dead volume was thus obtained through Eq. (1):

$$V_{\text{Void}} = V_2 - V_1. \tag{1}$$

After helium injection and degassing at the temperature of 200°C in vacuum, methane injection was performed. In order to determine the mole numbers of methane, Eqs. (2) and (3) were utilized:

$$n_{M,ini} = \frac{P_{M,ini}V}{Z_{M,ini}RT}, \tag{2}$$

$$n_{M,eq} = \frac{P_{M,eq}V}{Z_{M,eq}RT}, \tag{3}$$

in which $n_{M,ini}$ and $n_{M,eq}$ represent the initial and equilibrium mole numbers of methane, respectively. Furthermore, $Z_{M,ini}$ and $Z_{M,eq}$ represent the initial and equilibrium compressibility factors of methane before and after equilibrium, respectively. Thus, the total mole number of methane entered into the sample cell was determined through Eq. (4):

$$n_T = n_{M,eq} - n_{M,ini}. \tag{4}$$

Finally, the total mole of adsorbed methane was calculated through Eq. (5):

$$n_{\text{adsorbed}} = n_T - n_{\text{Void}}, \tag{5}$$

where, n_{Void} is the amount of gas in the dead volume calculated from Eq. (6):

$$n_{\text{Void}} = \frac{P_{M,eq}V_{\text{Void}}}{ZRT}. \tag{6}$$

Here, $P_{M,eq}$ is the equilibrium pressure of the system and V_{Void} is the corresponding dead volume.

3. Results and discussion

3.1. Characterization results

3.1.1. N₂ adsorption-desorption isotherms of the samples

In order to examine textural characteristics of the AC materials and effects of different synthesis parameters on them, nitrogen adsorption-desorption isotherms for all synthesized samples were determined; the results are presented in Figures 1 to 3. According to obtained results in this work, most samples were of type I in the IUPAC classification, showing the micro-porous structure of the materials. Moreover, some isotherms exhibited hysteresis, i.e. they contained both micro- and meso-pores. Figure 1 (with logarithmic scale) exhibits the N_2 isotherms obtained for four different samples at low relative pressures ($P/P_0 < 0.1$). The isotherms of the materials produced with hydrothermal treatment followed a classical type-I behavior, suggesting possession of a permanent micro-porous structure. However, for samples synthesized with no hydrothermal treatment, type-IV behavior was observed. The group-1 ACs (i.e., with hydrothermal treatment) presented a sigmoidal shaped N_2 adsorption behavior (see the logarithmic scale) corresponding to
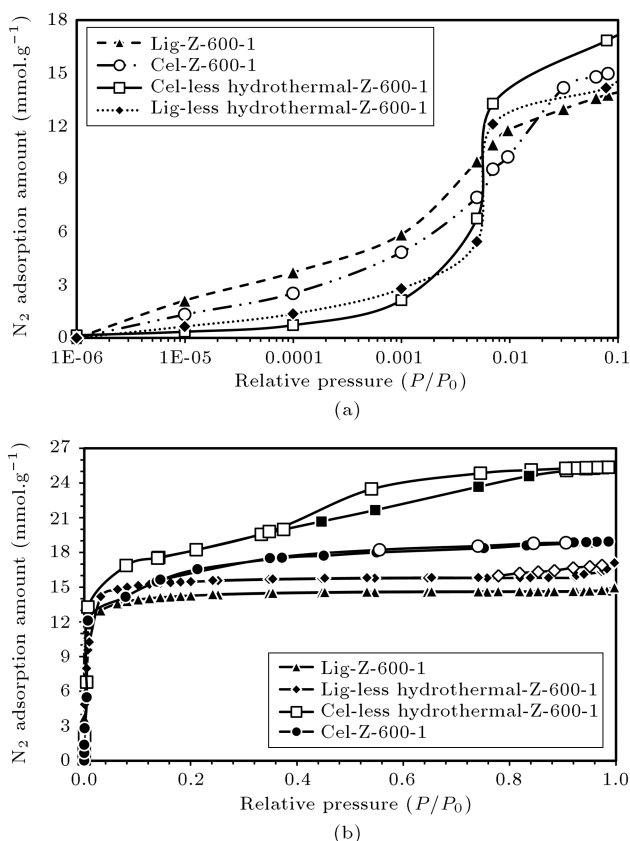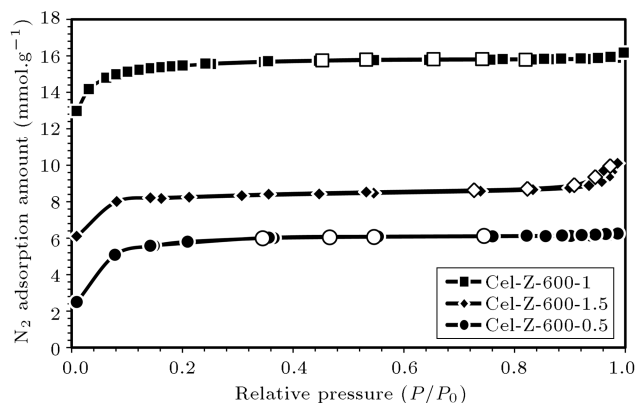
Figure 1. N_2 adsorption-desorption isotherms of activated carbons produced from cellulose and lignin with and without hydrothermal treatment of the precursors. Logarithmic-scale (a) and linear-scale (b). Filled symbols: adsorption, and empty symbols: desorption.
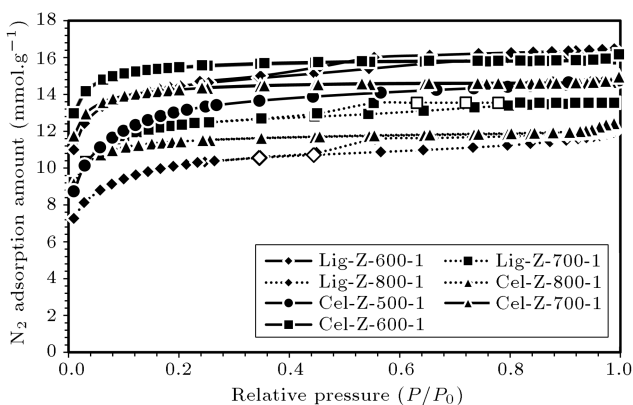
Figure 2. N_2 adsorption-desorption isotherms of activated carbons produced from cellulose and lignin at different carbonization temperatures in the present research. Filled symbols: adsorption, empty symbols: desorption.

strong adsorption of N_2 onto the pores. Consequently, pore fill-up was usually observed for smaller pore sizes. Moreover, the pressure range of micro-pore occupations increased with enhanced pore diameter of ACs in the group-2 materials (i.e., without hydrothermal treat-

Figure 3. N_2 adsorption-desorption isotherms of activated carbons produced from cellulose at 600°C with different impregnation ratios. Filled symbols: adsorption, and empty symbols: desorption.

ment). Thus, higher values of relative pressure (i.e., P/P_0) were observed for monolayer formation. Indeed, in group-2 ACs, significant sorption differences from group-1 were observed at higher relative pressures due to the multilayer formations or probably 2D condensations phenomenon.

Effects of precursor type and carbonization temperature on the textural properties

Textural characteristics of all synthesized samples are demonstrated in Table 1. One can observe that cellulose-based materials produced higher BET surface areas and total pore volumes than lignin-based ones did at all corresponding carbonization temperatures. Presence of more hydroxyl groups in the structure of cellulose caused higher amounts of volatile gaseous compounds released. This left behind higher surface area and pore volume in structure of the final product. On the other hand, presence of more carbon in the structure of lignin led to producing higher extents of micro-pores (i.e., V_{micro}/V_{total}) in the related samples.

On the other hand, higher carbonization temperatures produced higher V_{micro}/V_{total} and smaller average pore-diameters. However, for both cellulose and lignin-based materials, at carbonization temperatures above 700°C, the pore diameter increased while the V_{micro}/V_{total} ratio was lowered. At temperatures higher than 700°C, widening of the pores probably caused further pore development, leading to lowering of the micro-pore volume. Similar results were also reported for brown coal-based activated carbons and ACs prepared from peach stone carbonized at 850 and 900°C, respectively [21].

Effect of hydrothermal treatment on the textural properties

According to the results of Table 1, the samples produced from cellulose and lignin haydrochars revealed lower BET surface areas than those with no hydrother-

Table 1. Textural characteristics of the prepared activated carbons from cellulous and lignin impregnated with different agent/precursor ratios and activated at different carbonization temperatures in this work.

Sample ID	Precursor type	Activating agent	Carbonization temperature (°C)	Impregnation ratio	D_{ave} (BJH) (Å)	V_{micro} (cm^3/g)	V_{total} (cm^3/g)	S_{BET} (m^2/g)
Cel-Z-500-1	Cellulose	$ZnCl_2$	500	1	20.88	0.24	0.50	1011
Cel-Z-600-1	Cellulose	$ZnCl_2$	600	1	20.68	0.41	0.73	1293
Cel-Z-700-1	Cellulose	$ZnCl_2$	700	1	19.90	0.43	0.62	1091
Cel-Z-800-1	Cellulose	$ZnCl_2$	800	1	21.14	0.33	0.52	889
Lig-Z-600-1	Lignin	$ZnCl_2$	600	1	19.34	0.37	0.56	1100
Lig-Z-700-1	Lignin	$ZnCl_2$	700	1	18.95	0.32	0.46	956
Lig-Z-800-1	Lignin	$ZnCl_2$	800	1	19.63	0.28	0.41	782
Cel-Z-600-1.5	Cellulose	$ZnCl_2$	600	1.5	24.18	−	0.33	562
Cel-Z-600-0.5	Cellulose	$ZnCl_2$	600	0.5	22.10	−	0.27	383
Cel-less hydrothermal-Z-600-1	Cellulose	$ZnCl_2$	600	1	26.61	0.38	0.87	1371
Lig-less hydrothermal-Z-600-1	Lignin	$ZnCl_2$	600	1	24.43	0.31	0.65	1178

mal treatment. Besides, the total pore volumes (V_{total}) of the samples produced with no hydrothermal processing were higher than those of their hydrothermal counterpart. Nonetheless, their V_{micro}/V_{total} ratios were rather low. This might be due to the sudden release of volatile functional groups such as $-OH$, $-C=O$, $-COOH$, and volatile components existing in the cellulose's and lignin's internal structure, leaving larger pores behind mainly of meso type.

Effect of impregnation ratio on the textural properties

The optimum amount of $ZnCl_2$ used as activating agent led to high methane adsorption in comparison with the virgin adsorbent. This was because of materials possessing higher BET surface areas and micro-pore volumes in addition to narrowing down the pore size distribution after incorporating the agent into the precursor. In the present study, the optimum impregnation ratio of 50 wt% activating agent to the precursor type was revealed to be 1. These results were in agreement with those of the N_2 adsorption-desorption isotherms for the samples presented in Figure 3.

3.1.2. TGA and DTGA graphs of lignin and cellulose
The TG and DTG analyses of cellulose, lignin, and optimum sample (cellulose impregnated with $ZnCl_2$ of impregnation ratio of 1 and carbonized at 600°C) are presented in Figure 4(a)-(c). In the thermal decomposition profiles of cellulose and lignin (Figure 4(a) and (b)), a very distinct peak was observed at temperatures

between 30 and 100°C, which was related to the release of physisorbed water. However, a significant peak was observed at 300-400°C and attributed to the degradation of cellulose and lignin structures. In the current research, the DTGA peaks were at 366°C for the cellulose and 326°C for the lignin, both in acceptable agreement with previous work done by other researchers [22] reporting the DTGA peaks of 350°C for cellulose and 315°C for lignin. In this study, the final yield of lignin was higher than that of cellulose due to more volatility of the structure of cellulose. According to Figure 4(c), in the cel-Z-600-1 sample, the thermal decomposition occurred at several stages. From 50 to 400°C, the weight loss was due to the release of water and decomposition of cellulose (happening at temperatures lower than 365°C). It means that $ZnCl_2$ proceeded to decompose the cellulose at low temperatures, hence limiting the char formation [23]. Then, a significant weight loss occurred at about 520°C in the main activation. This was due to the main porosity formed in the space left behind by the $ZnCl_2$ species after being washed away with distilled water and acid, rather than volatilization of the material at its boiling point of 732°C [24].

3.1.3. FESEM images of the prepared ACs
Figure 5 presents the FESEM images of some selected AC samples synthesized in this research, revealing their morphologies. It indicates that the external surfaces of ACs prepared from cellulose and lignin activated with $ZnCl_2$ were full of cavities resulting from
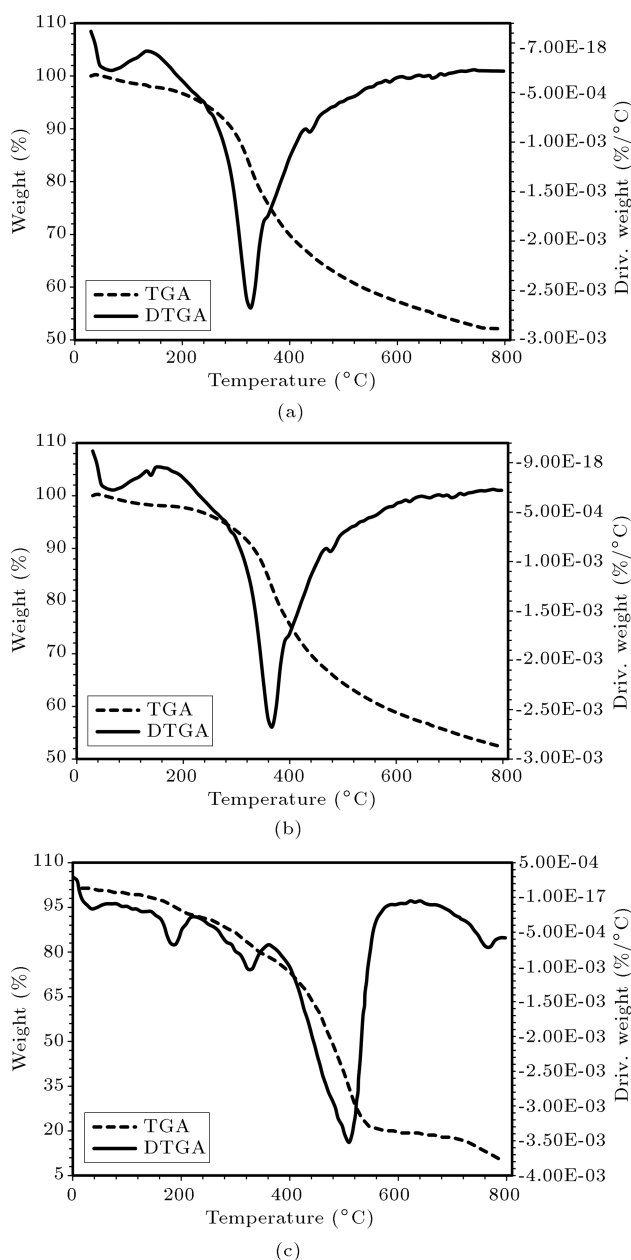
Figure 4. TGA and DTGA curves of (a) lignin, (b) cellulose, and (c) optimum sample (cel-Z-600-1) prepared in this research.

washing with distillated water and acid. Moreover, vaporization of volatile components existing in the internal structure of the samples such as OH, CO, and CO_2 functional groups and the Cl_2 gas molecules due to the $ZnCl_2$ species led to this structure. These results were consistent with those obtained by other researchers [25].

3.2. Methane adsorption experimental data
3.2.1. Effects of the precursor type
This study revealed that, as a precursor for preparing ACs, cellulose led to materials with higher methane adsorption capacities than lignin did. In addition, the lignin-based samples possessed lower textural characteristics, such as BET surface area and V_{total}, than cellulose-based ones, leading to lower methane adsorption capacities. It is noteworthy that, in general, effective micro-pore size of the adsorbent should be three to six times higher than that of the adsorbate. Thus, for an adsorbate methane molecule with a diameter of 0.38 nm, a material with pore diameters ranging from 1.2 to 2.2 nm is considered to be suitable as an adsorbent. Table 1 indicated that pore diameters of synthesized ACs in this research were well within this range.

3.2.2. Hydrothermal treatment
According to the results presented in Figures 6 and 7, hydrothermal treatment affected methane adsorption capacities positively for both cellulose- and lignin-based materials. In other words, in case of cellulose-based sorbent, methane adsorption capacity was enhanced from 4.05 to 6.34 $mmol.g^{-1}$ and, in case of lignin-based sorbent, it increased from 3.75 to 5.12 $mmol.g^{-1}$ at 298 K and 3.8 MPa.

3.2.3. Carbonization temperature
Figures 8 and 9 provide information on the carbonization temperature effects on the methane adsorption.

It was noteworthy that creating the initial porosity and enriching the carbon content of the precursor were the purposes of carbonization. According to the results of the textural characteristics exhibited in Table 1, 600°C was the optimum carbonization temperature at which such properties of both types of samples (i.e., lignin- and cellulose-based) were at their best positions, leading to the highest methane adsorption on cel-Z-600-1 and lig-Z-600-1 samples. In other words, the methane adsorption capacities of cel-Z-600-1 and lig-Z-600-1 species were determined to be 6.42 and 5.06 $mmol.g^{-1}$ at 298 K and 3.65 MPa, respectively.

3.2.4. Impregnation ratio
Influence of the impregnation ratio on methane adsorption is displayed in Figure 10.

Based upon the results presented in Table 1, amongst all three synthesized cellulose-based samples, the "cel-Z-600-1" with impregnation ratio of 1 exhibited the optimum textural properties, including the highest specific surface area as well as relatively high micro- and total pore volumes. Moreover, this led to the highest methane adsorption capacities throughout the considered range of pressures at 298 K (please see Figure 10).

3.2.5. CH_4 equilibrium adsorption modeling
Investigation into the adsorption thermodynamics of the studied systems was carried out through applying three different adsorption isotherms. The objective
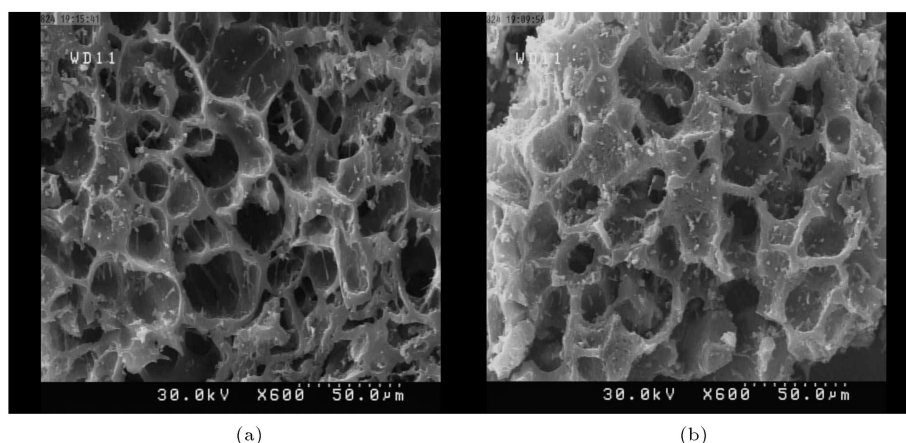
(a)   (b)

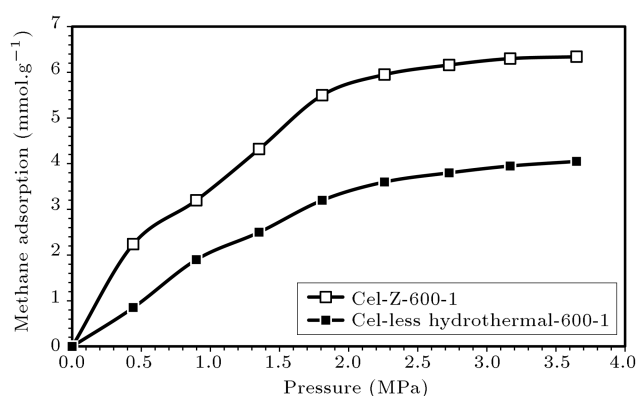**Figure 5.** FESEM images of (a) cel-Z-600-1:1 and (b) lig-Z-600-1:1 synthesized in this work.

Figure 6. Adsorption isotherms of methane on cel-Z-600-1 and cel-less hydrothermal-Z-600-1 synthesized in this research.
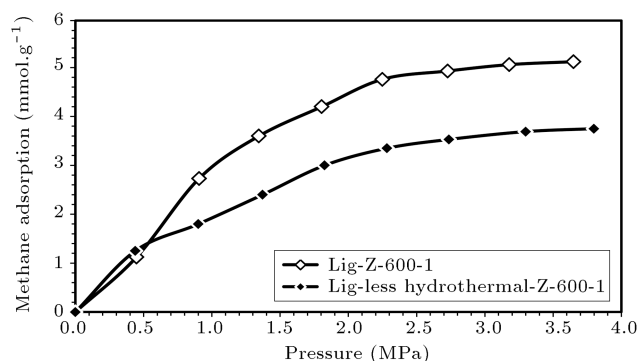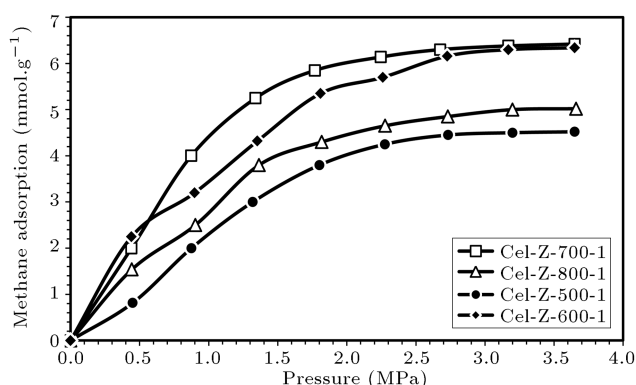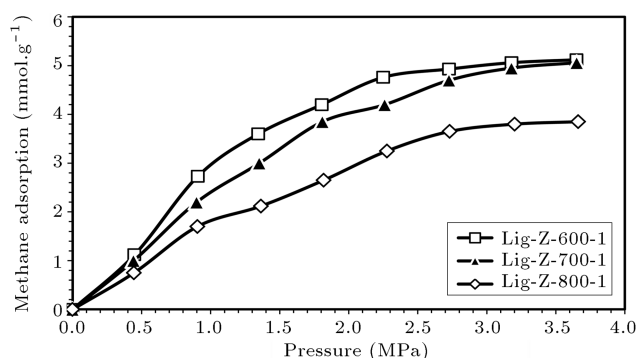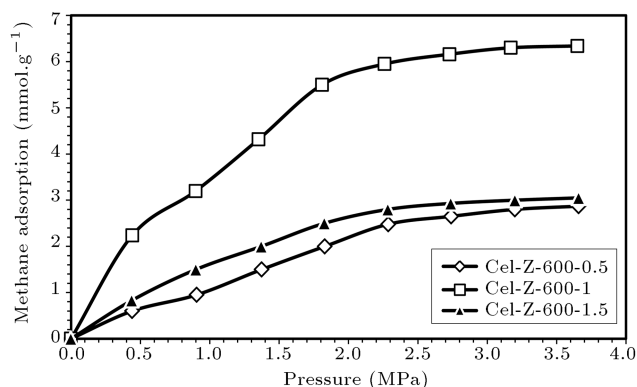

Figure 8. Adsorption isotherms of methane on prepared activated carbons from cellulose hydrochars at different carbonization temperatures of 500, 600, 700, and 800°C with impregnation ratio of 1 made in this work.

Figure 7. Adsorption isotherms of methane on lig-Z-600-1 and lig-less hydrothermal-Z-600-1 synthesized in this research.

Figure 9. Adsorption isotherms of methane on prepared activated carbons from lignin hydrochars at different carbonization temperatures of 600, 700, and 800°C with impregnation ratio of 1 made in this work.

was to determine which model might describe the adsorption process more accurately. Langmuir (Eq. (7)), Freundlich (Eq. (8)), and Sips (Eq. (9)) equations were chosen to analyze the experimental data in this work. The following relations provided these models:

$$q = \frac{q_m.b.P}{1 + b.P},$$ (7)

$$q = K_F P^{1/n},$$ (8)
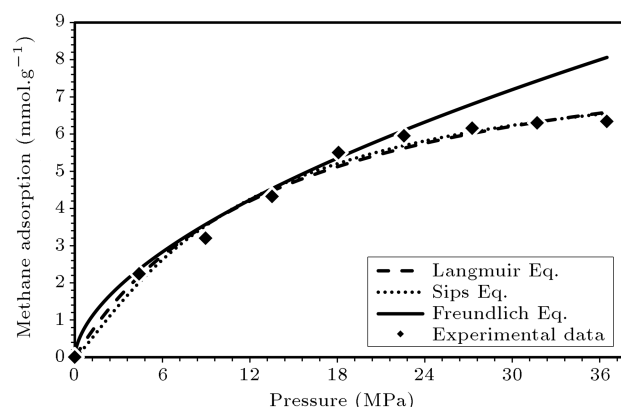
$$q = \frac{q_m.(K.P)^{1/n}}{1 + (K.P)^{1/n}},$$ (9)

where q_m (mmol.g^{-1}) is a Langmuir parameter related to the maximum adsorption capacity of methane

Figure 10. Adsorption isotherms of methane on activated carbons produced from cellulose hydrochars at 600°C with different impregnation ratios of 0.5, 1, and 1.5 prepared in this study.

Figure 11. Comparison of theoretical adsorption isotherms using the Langmuir, Freundlich, and Sips models with experimental data for the cel-Z-600-1 sample in this research.

on the prepared activated carbons and b (MPa^{-1}) is a Langmuir parameter related to the intensity of methane adsorption. K_F $(\text{mmol.g}^{-1}.\text{MPa}^{-1/n})$ is the Freundlich constant and n is surface heterogeneity parameter of the solid. The constant K_F is an approximate indication of the adsorption capacity, while $1/n$ is a function of the strength of adsorption [26]. However, K_F and n are characteristic parameters of the sorbent-sorbate system that should be determined through fitting with the experimental data. The model parameters with correlation coefficient, R^2, are represented in Table 2 and the simulated isotherms by the Langmuir, Freundlich, and Sips models are shown in Figure 11. Here, the data for the optimum cel-Z-600-1 sample are demonstrated.

As shown in Table 2, for some samples, the n

value was greater than 1, indicating that the adsorption was cooperative and the surface should not be assumed homogeneous; both were consistent with results of other researchers [27]. In addition, the value of q_m, indicating the maximum adsorption capacity, was higher for the sample produced from cellulose than for that from lignin-hydrochars. This might be due to the higher BET surface areas and total pore volumes as well as acceptable micro-pore volumes of the samples prepared from cellulose. In addition, the value of K_F (i.e., the intensity of adsorption) for the samples produced from cellulose and lignin hydrochars at 600°C with impregnation ratio of 1 was superior.

One can observe in Table 2 that Sips, as a combination of Langmuir and Freunlich models, ex-

Table 2. Isotherm constants of Langmuir, Freundlich, and Sips models for methane adsorption by activated carbons at 298K according to the experimental data of the current paper.

Sample ID	Langmuir				Freundlich				Sips				
	q_m	b	R^2	r_s	K_F	n	R^2	r_s	q_m	b	n	R^2	r_s
Cel-Z-500-1	6.385	1.050	0.937	0.922	5.190	1.324	0.962	0.922	5.770	1.060	1.523	0.993	0.989
Cel-Z-600-1	9.124	0.710	0.976	0.934	5.800	1.005	0.987	0.958	8.137	0.890	1.213	0.990	0.987
Cel-Z-700-1	7.961	1.290	0.968	0.939	4.580	1.045	0.957	0.941	6.749	1.420	1.953	0.997	0.998
Cel-Z-800-1	5.858	0.960	0.914	0.911	4.950	1.474	0.953	0.936	5.752	0.840	1.362	0.986	0.975
Lig-Z-600-1	6.635	0.950	0.924	0.936	5.360	1.423	0.952	0.933	5.894	1.010	1.525	0.998	0.999
Lig-Z-700-1	6.578	0.820	0.905	0.928	5.160	1.481	0.962	0.968	7.691	0.530	1.072	0.997	0.992
Lig-Z-800-1	5.076	0.780	0.920	0.946	4.530	1.866	0.928	0.957	8.604	0.220	0.082	0.994	0.996
Cel-Z-600-0.5	3.599	0.890	0.861	0.935	4.600	3.536	0.785	0.897	5.194	0.360	0.965	0.995	0.999
Cel-Z-600-1.5	4.101	0.810	0.927	0.941	4.740	2.956	0.820	0.901	3.747	0.860	1.423	0.996	0.999
Cel-less hydrothermal-Z-600-1	5.089	0.960	0.881	0.905	4.930	1.959	0.914	0.938	5.406	0.700	1.242	0.996	0.998
Lig-less hydrothermal-Z-600-1	4.512	1.660	0.920	0.937	4.380	1.704	0.940	0.955	5.315	0.650	1.054	0.992	0.997

plained the studied adsorption with a very satisfying $R^2 (> 0.99)$ in all experimental points. The Spearman's correlation coefficient (r_s), which is generally used in assessing the global correlation and dispersion of its relative errors, was applied in the current work to evaluate statistical acceptance. Eq. (10) represents this error function:

$$r_s = 1 - \frac{6 \sum_{i=1}^{n} (q_{exp,i} - q_{cal,i})^2}{n(n-1)^2}, \tag{10}$$

where n is the number of the experimental data, and q_{exp} (mmol.g^{-1}) and q_{cal} (mmol.g^{-1}) are the amounts of experimental and calculated adsorbed methane on the activated carbon surfaces through the adsorption isotherm model, respectively. It should be noted that as the value of r_s becomes closer to 1, the relative error of the equation is lowered; hence, it becomes more precise. Thus, based upon the values of error indicators presented in Table 2, the Sips model was chosen as the best one for describing adsorption of methane on the prepared activated carbons.

3.2.6. CH₄ adsorption kinetic modeling
Kinetic investigations always provide significant information about the mechanism of a given process. Hence, to examine the mechanism of adsorption in this research, the CH$_4$ adsorption on the optimum sample (cel-Z-600-1) was studied as a function of time. The obtained results are demonstrated in Figure 12.

As indicated in this figure, CH$_4$ sorption was rather rapid during the first 30 s and, afterwards, it steadily continued to increase until equilibrium was achieved. Most probably, in the first 10-30 s, the CH$_4$ molecules contacted external surfaces of the sorbents. Next, these molecules diffused into the AC's pores and were adsorbed on its internal surfaces. In other words, initially, the reactive-adsorptive sites on the external surfaces of the sorbent led to a rather intensive adsorption. Then, it was followed by a slow diffusion
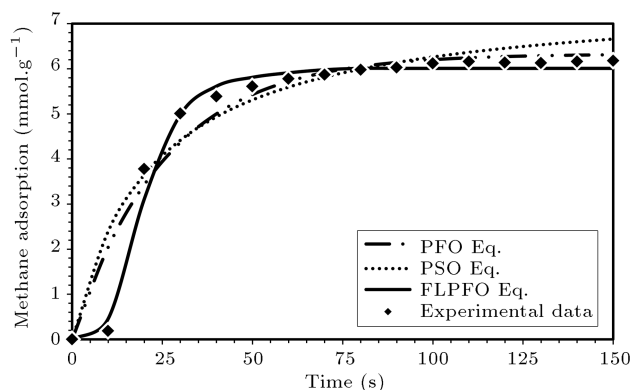
Figure 12. Effect of the contact time on the adsorption of CH$_4$ at 4 MPa and 298 K on the cel-Z-600-1 sample prepared in this work (the symbols show the experimental data).

process. The experimental data were compared with several kinetic models including PFO (Pseudo First Order), PSO (Pseudo Second Order), and FL-PFO (Fractal-Like Pseudo First Order). The adjustable parameters with corresponding coefficient of determination, R^2, and Spearman's correlation coefficient, r_s, are exhibited in Table 4. The fitted kinetic models with experimental data are further demonstrated in Figure 12. Again, α is the parameter related to the heterogeneity of the adsorbent's surface and is often determined to be greater than 1, indicating the complexity of the adsorbent-adsorbate interactions. It should be noted that k_i $(i = 1, 2)$ was the kinetic constant of the aforementioned models due to the initial methane adsorption (e.g., during the first 30 s) on the external surfaces of the sorbents until reaching an equilibrium plateau. In fact, greater values of k_i might result in greater extent of initial adsorptions. As it can be observed in Table 3 and according to the more accurate kinetic model of FL-PFO (based upon the related values of R^2 and r_s), the values of k_i were lowered due to decrease in the BET surface area of the materials considered (please see Table 1). Hence, it could be predicted that the sorbents possessing higher specific surface areas would lead to more pronounced initial adsorption. Figure 12 as well as the data provided in Table 3 show that the FL-PFO kinetic model theoretically best fitted the obtained experimental data due to its one more adjustable parameter than the other models utilized in this work.

3.2.7. A comparison between the current and recent CH₄ adsorptions
Table 4 represents the CH$_4$ adsorption capacity of some carbon-based adsorbents under a wide range of operating conditions of temperature and pressure. The data were prepared under different synthesis conditions of carbonization temperatures and types of activating agent. It became evident that, for the majority of cases, the carbonaceous adsorbents prepared in this work adsorbed higher amounts of CH$_4$ than their open-literature counterparts under the same conditions. Satisfactory performances of the obtained optimum adsorbents in the current study (i.e., cel-Z-600-1 and lig-Z-600-1 samples) were due to the combination of three major factors, including the hydrothermal pre-treatment, carbonization temperature, and ratio of a prevalent activating agent to the AC materials.

4. Conclusion

The hydrothermal pretreatment of cellulose and lignin species made highly micro-porous volumes and narrow pore diameter distribution of around 2 nm suitable for methane adsorption. Carbonizing at optimum temperature further allowed for development of micro-

Table 3. Adjustable parameters to adsorption kinetic equations at 298 K studied in this research.

Kinetic model	Adsorbent	q_{cal} (mmol.g^{-1})	k_1 (min^{-1})	k_2 (min^{-1})	α	R^2	r_s
Pseudo-first-order $q_t = q_e.(1 - exp(-k_1 t))$	Cel-Z-500-1	4.561	0.028	–	–	0.926	0.964
	Cel-Z-600-1	6.329	0.039	–	–	0.905	0.955
	Cel-Z-700-1	6.705	0.024	–	–	0.852	0.927
	Cel-Z-800-1	5.232	0.025	–	–	0.903	0.908
	Lig-Z-600-1	5.255	0.030	–	–	0.897	0.913
	Lig-Z-700-1	5.302	0.026	–	–	0.893	0.907
	Lig-Z-800-1	3.940	0.031	–	–	0.925	0.926
	Cel-Z-600-0.5	2.993	0.033	–	–	0.973	0.978
	Cel-Z-600-1.5	3.124	0.039	–	–	0.936	0.969
	Cel-less hydrothermal-Z-600-1	4.135	0.042	–	–	0.871	0.904
	Lig-less hydrothermal-Z-600-1	3.840	0.039	–	–	0.906	0.918
Pseudo-second-order $q_t = \frac{k_2 q_e^2 t}{1 + k_2 q_e t}$	Cel-Z-500-1	5.931	–	0.005	–	0.882	0.897
	Cel-Z-600-1	7.629	–	0.006	–	0.784	0.846
	Cel-Z-700-1	8.499	–	0.003	–	0.758	0.820
	Cel-Z-800-1	6.770	–	0.003	–	0.871	0.869
	Lig-Z-600-1	6.641	–	0.004	–	0.825	0.886
	Lig-Z-700-1	6.805	–	0.004	–	0.845	0.871
	Lig-Z-800-1	4.982	–	0.006	–	0.898	0.819
	Cel-Z-600-0.5	3.577	–	0.010	–	0.931	0.944
	Cel-Z-600-1.5	3.796	–	0.011	–	0.894	0.965
	Cel-less hydrothermal-Z-600-1	4.935	–	0.009	–	0.836	0.865
	Lig-less hydrothermal-Z-600-1	5.025	–	0.008	–	0.789	0.859
Fractal like-pseudo-first-order $q_t = q_e.(1 - exp(-k_1 t^\alpha))$	Cel-Z-500-1	4.366	0.052	–	1.588	0.971	0.986
	Cel-Z-600-1	6.009	0.093	–	2.170	0.901	0.968
	Cel-Z-700-1	6.176	0.066	–	1.677	0.977	0.989
	Cel-Z-800-1	4.826	0.048	–	1.518	0.974	0.982
	Lig-Z-600-1	4.947	0.078	–	1.734	0.968	0.977
	Lig-Z-700-1	4.924	0.053	–	1.780	0.987	0.992
	Lig-Z-800-1	3.693	0.036	–	1.775	0.981	0.991
	Cel-Z-600-0.5	2.709	0.037	–	2.201	0.979	0.988
	Cel-Z-600-1.5	2.988	0.033	–	2.349	0.996	0.999
	Cel-less hydrothermal-Z-600-1	3.968	0.072	–	2.210	0.975	0.990
	Lig-less hydrothermal-Z-600-1	3.672	0.059	–	2.289	0.994	0.998

pores on the internal structure of samples. Moreover, effects of ZnCl$_2$ as the activating agent and influences of different parameters on the textural and structural properties as well as methane storage capacities of produced ACs were investigated. It was revealed that both carbonization temperature and impregnation ratio had great effects on textural quality of the final products. In addition, optimum temperature and impregnation ratio resulted in a product with a high BET surface area, micro-porous volume, and appropriate pore diameter size for methane adsorption. Moreover, the AC materials produced from cellulose, carbonized at 600°C, and activated by ZnCl$_2$ with the impregnation ratio of 1 provided the highest capacity for methane storage, which amounted to 6.42 mmol.g^{-1} due to the highest V_{micro}/V_{total} ratio, suitable average pore diameter, and considerable specific surface area. Amongst several models considered, the Sips isotherm

Table 4. CH$_4$ adsorption capacities of some carbon-based adsorbents for comparison.

Material	Precursor	Synthesis conditions			CH$_4$ adsorption amount (mmol.g^{-1})				Reference
		Hydrothermal pretreatment	Carbonization temperature (°C)	Activating agent	$P = 1$ MPa	$P = 2$ MPa	$P = 3$ MPa	$P = 4$ MPa	
					T = 298 K	T = 298 K	T = 298 K	T = 298 K	
AC	Sorghum	No	300	H$_3$PO$_4$	2.74	4.11	4.65	5.02	[28]
AC	Wheat	No	300	H$_3$PO$_4$	2.32	3.74	4.21	4.48	[28]
AC	Oil palm shell	No	850	CO$_2$ (physical activation)	2.85	4.23	4.77	5.16	[29]
AC	Oil palm shell	No	850	ZnCl$_2$	2.69	4.05	4.54	4.96	[29]
Ac	Oil palm shell	No	850	H$_3$PO$_4$	2.81	4.14	4.70	5.08	[29]
AC	Corn cobs	No	550	KOH	2.25	3.69	4.17	4.39	[30]
AC	Palm shell	No	855	H$_3$PO$_4$	2.95	4.38	4.86	5.25	[31]
AC	Coconut shell	No	No	ZnCl$_2$	2.12	3.16	3.95	4.21	[32]
AC	Cellulose	No	800	CO$_2$ (physical activation)	3.12	4.89	5.32	5.68	[33]
AC	Sugarcane molasses	No	800	KOH	4.26	5.89	7.96	8.24	[34]
AC	Cellulose	Yes	600	ZnCl$_2$	3.15	5.13	6.18	6.45	This work
AC	Lignin	Yes	600	ZnCl$_2$	2.95	4.42	4.96	5.16	This work

satisfyingly fitted the determined experimental data. This led to the conclusion that the nature of the sorbents surfaces considered was heterogeneous. Then, the kinetics of CH$_4$ adsorption on the prepared ACs were studied. Considering several kinetic models revealed that the FL-PFO equation satisfyingly described this system with a goodness of fit of above 97%. In this regard, the adsorption constants demonstrated to be time dependent, which was considered as a consequence of the aforementioned surface heterogeneity of the synthesized materials.

References

1. Rios, R.B., Bastos-Neto, M., Amora Jr, M.R., Torres, A.E.B., Azevedo, D.C., and Cavalcante Jr, C.L. "Experimental analysis of the efficiency on charge/discharge cycles in natural gas storage by adsorption", *Fuel*, **90**(1), pp. 113-119 (2011).

2. Prauchner, M.J. and Rodriguez-Reinoso, F. "Preparation of granular activated carbons for adsorption of natural gas", *Microporous and Mesoporous Materials*, **109**(1-3), pp. 581-584 (2008).

3. Gholipour, F. and Mofarahi, M. "Adsorption equilibrium of methane and carbon dioxide on zeolite 13X: Experimental and thermodynamic modeling", *The Journal of Supercritical Fluids*, **111**, pp. 47-54 (2016).

4. Yeganegi, S. and Gholampour, F. "Simulation of methane adsorption and diffusion in a carbon nanotube channel", *Chemical Engineering Science*, **140**, pp. 62-70 (2016).

5. Shen, J., Sulkowski, J., Beckner, M., and Dailly, A. "Effects of textural and surface characteristics of metal-organic frameworks on the methane adsorption for natural gas vehicular application", *Microporous and Mesoporous Materials*, **212**, pp. 80-90 (2015).

6. Blanco, A.A.G., Vallone, A.F., Korili, S.A., Gil, A., and Sapag, K. "A comparative study of several microporous materials to store methane by adsorption", *Microporous and Mesoporous Materials*, **224**, pp. 323-331 (2016).

7. Casco, M.E., Martinez-Escandell, M., Kaneko, K., Silvestre-Albero, J., and Rodríguez-Reinoso, F. "Very high methane uptake on activated carbons prepared from mesophase pitch: a compromise between microporosity and bulk density", *Carbon*, **93**, pp. 11-21 (2015).

8. Zhang, T., Walawender, W.P., and Fan, L.T. "Grain-based activated carbons for natural gas storage", *Bioresource Technology*, **101**(6), pp. 1983-1991 (2010).

9. Bagheri, N. and Abedi, J. "Adsorption of methane on corn cobs based activated carbon", *Chemical Engineering Research and Design*, **89**(10), pp. 2038-2043 (2011).

10. Matos, J., Nahas, C., Rojas, L., and Rosales, M. "Synthesis and characterization of activated carbon from sawdust of Algarroba wood. 1. Physical activation and pyrolysis", *Journal of Hazardous Materials*, **196**, pp. 360-369 (2011).

11. Khezami, L., Chetouani, A., Taouk, B., and Capart, R. "Production and characterisation of activated carbon from wood components in powder: cellulose, lignin, xylan", *Powder Technology*, **157**(1-3), pp. 48-56 (2005).

12. Cagnon, B., Py, X., Guillot, A., Stoeckli, F., and Chambat, G. "Contributions of hemicellulose, cellulose and lignin to the mass and the porous properties of chars and steam activated carbons from various ligno-cellulosic precursors", *Bioresource Technology*, **100**(1), pp. 292-298 (2009).

13. Dastgheib, S.A. and Rockstraw, D.A. "Pecan shell activated carbon: synthesis, characterization, and application for the removal of copper from aqueous solution", *Carbon*, **39**(12), pp. 1849-1855 (2001).

14. Sun, M. and Hong, L. "Impacts of the pendant functional groups of cellulose precursor on the generation of pore structures of activated carbons", *Carbon*, **49**(7), pp. 2173-2180 (2011).

15. Sevilla, M. and Fuertes, A.B. "The production of carbon materials by hydrothermal carbonization of cellulose", *Carbon*, **47**(9), pp. 2281-2289 (2009).

16. Roman, S., Nabais, J.V., Ledesma, B., González, J.F., Laginhas, C., and Titirici, M.M. "Production of low-cost adsorbents with tunable surface chemistry by conjunction of hydrothermal carbonization and activation processes", *Microporous and Mesoporous Materials*, **165**, pp. 127-133 (2013).

17. Lu, X., Pellechia, P.J., Flora, J.R., and Berge, N.D. "Influence of reaction time and temperature on product formation and characteristics associated with the hydrothermal carbonization of cellulose", *Bioresource Technology*, **138**, pp. 180-190 (2013).

18. Demiral, H., Demiral, I., Tümsek, F., and Karabacakoğlu, B. "Pore structure of activated carbon prepared from hazelnut bagasse by chemical activation", *Surface and Interface Analysis*, **40**(3-4), pp. 616-619 (2008).

19. Rodriguez-Reinoso, F. and Molina-Sabio, M. "Activated carbons from lignocellulosic materials by chemical and/or physical activation: an overview", *Carbon*, **30**(7), pp. 1111-1118 (1992).

20. Pourebrahimi, S., Kazemeini, M., Babakhani, E.G., and Taheri, A. "Removal of the CO_2 from flue gas utilizing hybrid composite adsorbent MIL-53 (Al)/GNP metal-organic framework", *Microporous and Mesoporous Materials*, **218**, pp. 144-152 (2015).

21. Carrott, P.J.M. and Carrott, M.R. "Lignin-from natural adsorbent to activated carbon: a review", *Bioresource Technology*, **98**(12), pp. 2301-2312 (2007).

22. Hu, J., Shen, D., Wu, S., Zhang, H., and Xiao, R. "Effect of temperature on structure evolution in char from hydrothermal degradation of lignin", *Journal of Analytical and Applied Pyrolysis*, **106**, pp. 118-124 (2014).

23. Uçar, S., Erdem, M., Tay, T., and Karagöz, S. "Preparation and characterization of activated carbon produced from pomegranate seeds by $ZnCl_2$ activation", *Applied Surface Science*, **255**(21), pp. 8890-8896 (2009).

24. Salame, I.I. and Bandosz, T.J. "Role of surface chemistry in adsorption of phenol on activated carbons", *Journal of Colloid and Interface Science*, **264**(2), pp. 307-312 (2003).

25. Caturla, F., Molina-Sabio, M., and Rodriguez-Reinoso, F. "Preparation of activated carbon by chemical activation with $ZnCl_2$", *Carbon*, **29**(7), pp. 999-1007 (1991).

26. Pourebrahimi, S., Kazemeini, M., and Vafajoo, L. "Embedding graphene nanoplates into MIL-101 (Cr) pores: Synthesis, characterization, and CO_2 adsorption studies", *Industrial & Engineering Chemistry Research*, **56**(14), pp. 3895-3904 (2017).

27. Arami-Niya, A., Daud, W.M.A.W., and Mjalli, F.S. "Comparative study of the textural characteristics of oil palm shell activated carbon produced by chemical and physical activation for methane adsorption", *Chemical Engineering Research and Design*, **89**(6), pp. 657-664 (2011).

28. Diao, Y., Walawender, W.P., and Fan, L.T. "Activated carbons prepared from phosphoric acid activation of grain sorghum", *Bioresource Technology*, **81**(1), pp. 45-52 (2002).

29. Arami-Niya, A., Daud, W.M.A.W., Mjalli, F.S., Abnisa, F., and Shafeeyan, M.S. "Production of microporous palm shell based activated carbon for methane adsorption: modeling and optimization using response surface methodology", *Chemical Engineering Research and Design*, **90**(6), pp. 776-784 (2012).

30. Bagheri, N. and Abedi, J. "Preparation of high surface area activated carbon from corn by chemical activation using potassium hydroxide", *Chemical Engineering Research and Design*, **87**(8), pp. 1059-1064 (2009).

31. Guo, J. and Lua, A.C. "Surface functional groups on oil-palm-shell adsorbents prepared by H_3PO_4 and KOH activation and their effects on adsorptive capacity", *Chemical Engineering Research and Design*, **81**(5), pp. 585-590 (2003).

32. Azevedo, D.C., Araujo, J.C.S., Bastos-Neto, M., Torres, A.E.B., Jaguaribe, E.F., and Cavalcante, C.L. "Microporous activated carbon prepared from coconut shells using chemical activation with zinc chloride", *Microporous and Mesoporous Materials*, **100**(1-3), pp. 361-364 (2007).

33. Himeno, S., Komatsu, T., and Fujita, S. "High-pressure adsorption equilibria of methane and carbon dioxide on several activated carbons", *Journal of Chemical & Engineering Data*, **50**(2), pp. 369-376 (2005).

34. Sreńscek-Nazzal, J., Kamińska, W., Michalkiewicz, B., and Koren, Z.C. "Production, characterization and methane storage potential of KOH-activated carbon from sugarcane molasses", *Industrial Crops and Products*, **47**, pp. 153-159 (2013).

Biographies

Sina Pourebrahimi received his BSc degree in Chemical Engineering from Isfahan University of Technology,

Isfahan, Iran, in 2012, and his MSc degree in Chemical Engineering from Sharif University of Technology, Tehran, Iran, in 2014. He performed his MSc thesis under the supervision of Prof. Mohammad Kazemeini. His research interests include adsorption, catalysis, and materials chemistry.

Mohammad Kazemeini is currently Professor of Chemical and Petroleum Engineering at Sharif University of Technology, Tehran, Iran. His current research interests include nanocatalysts (mostly CNT and CNF as well as carbonecous based) preparation, characterization and evaluation in the field of chemical engineering, and petroleum refining.

Maryam Zaroudi received her BSc degree in Chemical Engineering from Amirkabir University of Tech-

nology, Tehran, Iran, in 2012, and her MSc degree in the same field from Sharif University of Technology, Tehran, Iran, in 2014. She investigated methane adsorption on ACs in Research Institute of Petroleum Industry, Tehran, Iran. Her research mainly focuses upon gas adsorption and separation.

Hamid Reza Bozorgzadeh has been working at RIPI (Research Institute of Petroleum Industry) as a Faculty Member since 2002. He received his BSc degree from the Technische Fachhoch schule (TFH) of Berlin, Germany, in 1997, and PhD in Physical Chemistry from the University-Potsdamm, Germany, in 2002. His main research interests include synthesis of heterogeneous catalysts, adsorbents, their characterization, and determination of catalytic reaction mechanisms as well as adsorption processes.